

Dynamic personalities of proteins

Katherine Henzler-Wildman¹ & Dorothee Kern¹

Because proteins are central to cellular function, researchers have sought to uncover the secrets of how these complex macromolecules execute such a fascinating variety of functions. Although static structures are known for many proteins, the functions of proteins are governed ultimately by their dynamic character (or 'personality'). The dream is to 'watch' proteins in action in real time at atomic resolution. This requires addition of a fourth dimension, time, to structural biology so that the positions in space and time of all atoms in a protein can be described in detail.

Life is marked by change over time, and biologists explore this phenomenon by watching, for example, *Caenorhabditis elegans* developing from embryos into adults, mice running in a cage, and nerve cells firing. In search of how and why, biology arrived at the molecular level. Understanding protein function on an atomic level has been revolutionized by high-resolution X-ray crystallography, resulting in a surge in studies of structure–function relationships. The detail in these colourful structures flooding the covers of modern journals can be deceptive, suggesting that one unique structure, the 'folded state', is the final answer. Ironically, the dynamic nature of biology seems to have been forgotten at this microscopic level.

Physicists, however, will object to a static picture: they see proteins as soft materials that sample a large ensemble of conformations around the average structure as a result of thermal energy. A complete description of proteins requires a multidimensional energy landscape that defines the relative probabilities of the conformational states (thermodynamics) and the energy barriers between them (kinetics). In biology, this concept has recently gained traction, leading to an extension of the structure–function paradigm to include dynamics. To understand proteins in action, the fourth dimension, time, must be added to the snapshots of proteins frozen in crystal structures. A major obstacle is that it is not possible to watch experimentally individual atoms moving within a protein. Instead, sophisticated biophysical methods are needed to measure the physical properties from which the dynamics can be inferred.

In this review, we discuss how protein function is rooted in the energy landscape. The basic concepts and the biophysical methods are illustrated by several examples. To avoid past semantic confusion about the term protein dynamics, we define it as any time-dependent change in atomic coordinates. Protein dynamics thus includes both equilibrium fluctuations and non-equilibrium effects. The fluctuations observed at equilibrium seem to govern biological function in processes both near and far from equilibrium; therefore, we focus on these motions. Non-equilibrium effects are also called dynamical effects¹ (the source of confusion²), and they have a minimal effect on the overall rates of biological processes^{3,4}. Biological motors that convert chemical energy to mechanical energy^{5,6} are not discussed here.

The energy landscape

Although the idea of an energy landscape might be most familiar in the context of protein folding (for example, the folding funnel hypothesis)^{7–9}, this concept had already been applied to folded proteins more than 30 years ago by Frauenfelder and co-workers¹⁰. Using flash photolysis, they measured the kinetics of carbon monoxide and oxygen

rebinding to myoglobin as a function of temperature and ligand concentration¹⁰. Based on the observation of multiple energy barriers and non-exponential kinetics below a temperature of 230 K, an energy-landscape model was developed¹¹. Frauenfelder and colleagues insightfully connected this energy-landscape concept to myoglobin function and characterized the features of the landscape, including the heights of the barriers between energy wells and the existence of multiple conformational substates¹². Subsequent studies on myoglobin led to the idea that substates are in thermal equilibrium and that both solvent^{13–15} and ligands influence the landscape (Fig. 1a). At the glass transition temperature^{10,12}, an increase in anharmonic dynamics occurs in proteins, and this is interpreted as the protein no longer being trapped in a single energy well. This transition has recently been attributed to a solvent relaxation effect in the hydration shell of proteins¹⁶. Since these early studies, many more details of protein energy landscapes have been characterized as a result of advances in experimental and computational techniques (described later).

We divide our discussion based on the timescale of the dynamic processes (Fig. 1). It should be noted, however, that protein dynamics are characterized not only by the timescale of the fluctuations (a kinetic component) but also by the amplitude and the directionality of the fluctuations (a structural component). Consequently, the energy landscape representing a protein, which has many atoms, is highly multidimensional. It is also important to keep in mind that a particular energy landscape is tied to an individual set of temperature, pressure and solvent conditions. Manipulating these conditions is one of the most common ways to change the relative populations of the states and the kinetics of conversion between them. Logically, the energy landscape of a protein is inclusive of all the states sampled by the protein–solvent system, including the unfolded subspace. The process of protein folding, however, has been discussed thoroughly elsewhere (see refs 7–9, 17 and 18 for reviews) and is not covered here.

Slow timescales

Dynamics on a 'slow' timescale (tier-0 dynamics) define fluctuations between kinetically distinct states that are separated by energy barriers of several kT (the product of the Boltzmann constant and the absolute temperature), corresponding to timescales of microseconds and slower at physiological temperature. Typically, these are larger-amplitude collective motions between relatively small numbers of states. The protein is not static within one of these tier-0 states; instead, it fluctuates around the average structure on a faster timescale, exploring a large ensemble of closely related structures (see the section Fast timescales).

¹Department of Biochemistry, Howard Hughes Medical Institute, Brandeis University, Waltham, Massachusetts 02454, USA.

Transitions between tier-0 states are rare, however, owing to the low probability of the conformation that allows transition. Dynamics on this timescale have received much attention recently, because many biological processes — including enzyme catalysis, signal transduction and protein–protein interactions — occur on this timescale. Owing to the relatively long lifetimes of each state, these individual states can either be observed directly or be trapped experimentally. Moreover, the kinetics of interconversion of these states can also be detected. In this section, we discuss what has been learned about dynamics on slow timescales from experimental atomic-resolution methods, experimental low-resolution and local-site methods, and computational methods.

Experimental atomic-resolution methods

Ideally, researchers would like to determine both the structures of the tier-0 substates and their rates of interconversion. X-ray crystallography, nuclear magnetic resonance (NMR) spectroscopy, cryo-electron microscopy and small-angle X-ray scattering provide atomic-resolution or near-atomic-resolution snapshots of tier-0 substates. For high-resolution X-ray crystallography, a homogeneous crystal is needed. Consequently, substates need to be trapped through biochemical ‘tricks’, or the reaction needs to be synchronized across the entire crystal¹⁹. These ideas are nicely illustrated by the crystallographic characterization of intermediates in the cytochrome P450 enzymatic cycle²⁰.

The requirement for a homogeneous crystal is relieved when using cryo-electron microscopy and small-angle X-ray scattering, making it possible to determine the structural ensemble directly, in the experimental conditions, although with lower resolution. However, these methods cannot characterize the timescales of interconversion. Usually, this structural information is linked to kinetic data obtained from low-resolution spectroscopic methods (discussed in the next subsection, Experimental low-resolution and local-site methods). In specialized circumstances, both structures and kinetics can be determined simultaneously by using Laue X-ray diffraction¹⁹. In addition, hydrogen–deuterium exchange, analysed by either mass spectrometry or NMR spectroscopy, provides a particularly powerful way to detect global or local unfolding on timescales of milliseconds and longer^{21,22}.

The clear advantage of NMR methods is that they deliver the timescale of transitions, together with atomic resolution. Dynamic information is extracted from relaxation of nuclei after excitation, using a variety of NMR experiments to span dynamics on timescales from picoseconds to seconds and to assess several types of nucleus (¹H, ²H, ¹³C and ¹⁵N) site specifically^{23–25}. Importantly, the dynamics can be followed in solution in steady-state conditions²⁶. This is in contrast to most other spectroscopic methods, which require perturbation to measure kinetics. NMR experiments have traditionally been limited to small, soluble proteins. However, modern spectrometer technology (such as high magnetic fields and cryoprobes) and new NMR pulse sequences have pushed the size limit upward, making it possible to study proteins of up to 100 kDa and even up to the size of the ribosome, depending on the system and question of interest^{27–33}.

The NMR timescale for conformational exchange is defined by its rate (k_{ex} , the sum of the forward and reverse rates) relative to the chemical-shift timescale ($\Delta\omega$, the difference in chemical shift of the interconverting species). Interconversion is slow on the NMR timescale when $k_{ex} < \Delta\omega$, fast when $k_{ex} > \Delta\omega$, and intermediate when $k_{ex} \approx \Delta\omega$ (ref. 25). For a slow exchange rate, the substates are observed as distinct peaks in the spectrum, allowing direct structural characterization. The relative populations of the substates (p_A and p_B) are obtained from the relative peak integrals, and exchange rates from one-tenth of a second to tens of seconds can be measured by nuclear Overhauser enhancement spectroscopy (NOESY) and ZZ-exchange spectroscopy²⁴. By contrast, at intermediate and fast exchange rates, a single population-averaged signal is obtained. Microsecond-to-millisecond dynamics cause additional line broadening of this signal by an amount, R_{ex} , that contributes to the measured overall transverse relaxation rate (R_{2eff}). Specialized relaxation dispersion experiments^{24,25,34} have been developed, allowing

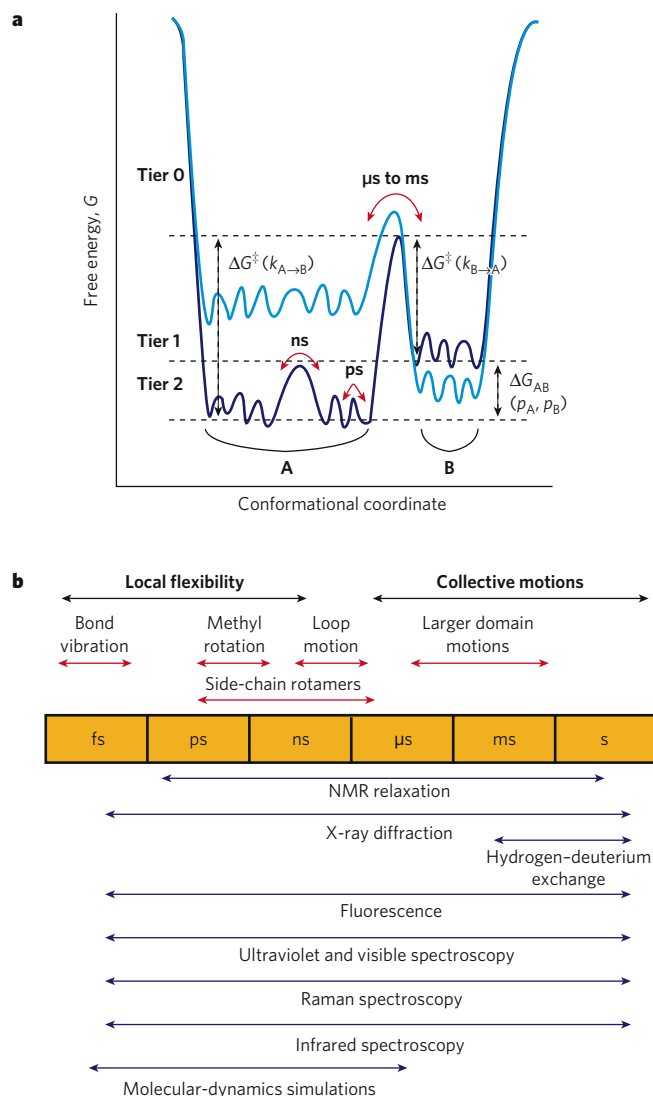


Figure 1 | The energy landscape defines the amplitude and timescale of protein motions. a, One-dimensional cross-section through the high-dimensional energy landscape of a protein showing the hierarchy of protein dynamics and the energy barriers. Each tier is classified following the description introduced by Frauenfelder and co-workers²³. A state is defined as a minimum in the energy surface, whereas a transition state is the maximum between the wells. The populations of the tier-0 states A and B (p_A , p_B) are defined as Boltzmann distributions based on their difference in free energy (ΔG_{AB}). The barrier between these states (ΔG^\ddagger) determines the rate of interconversion (k). Lower tiers describe faster fluctuations between a large number of closely related substates within each tier-0 state. A change in the system will alter the energy landscape (from dark blue to light blue, or vice versa). For example, ligand binding, protein mutation and changes in external conditions shift the equilibrium between states. **b**, Timescale of dynamic processes in proteins and the experimental methods that can detect fluctuations on each timescale.

determination of k_{ex} (kinetics), p_A and p_B (thermodynamics) and $\Delta\omega$ (structure) from the dependence of R_{ex} on an applied effective magnetic field (ν_{CPMG}) (Fig. 2a).

Using these dispersion experiments, the protein dynamics in an enzyme during catalysis have been measured, for cyclophilin A (CYPA)^{35,36} (Fig. 2). CYPA catalyses the reversible *cis*–*trans* isomerization of prolyl peptide bonds. It was originally identified as the target of the immunosuppressive drug cyclosporin A^{37,38}. Since then, peptidylprolyl isomerases have emerged as important regulators of various biological processes. For such a reversible enzyme, catalysis can be maintained indefinitely in the sample tube by simply adding the substrate(s)²⁶. Quantitative analysis of the NMR dispersion experiments on CYPA^{34,39,40}

revealed a global conformational exchange process that coincides with the chemical step of peptidylprolyl isomerization of the substrate on the enzyme³⁶ (Fig. 2a, b). The dynamics of individual microscopic steps of the catalytic cycle were dissected (that is, binding and dissociation, and isomerization)³⁵, and the collective nature of motions in a large dynamic network was experimentally characterized by studying proteins with various mutations³⁶ (Fig. 2d). Strikingly, characteristic motions detected during catalysis are already present in the free enzyme with frequencies similar to the turnover numbers (the number of molecules of substrate converted to product by one enzyme site per second)³⁶ (Fig. 2c). Therefore, the dynamics are an intrinsic property of the enzyme that is 'harvested' for catalytic turnover³⁶. We propose that this fundamental finding that free CYPA 'pre-samples' the conformational substates observed during catalysis might be a general paradigm for enzymes.

Experimental low-resolution and local-site methods

In the era of atomic-resolution methods, the classical biophysical techniques of fluorescence, circular dichroism, absorbance, infrared spectroscopy, Raman spectroscopy and electron paramagnetic resonance have been treated as second-class citizens. However, these time-honoured methods are now having a renaissance, owing to an appreciation of their power to provide kinetic information that is complementary to higher-resolution methods. These lower-resolution methods access a large range of timescales (Fig. 1b) with high precision, while providing information for one or a few sites or an average over the entire system.

Here, we focus on one new and exciting area in this category, the application of fluorescence at the single-molecule level^{41–44}. This technique brings to life a dream that biochemists have had for many years — watching a single protein molecule functioning in real time. The observed lifetimes of these states typically follow statistical exponential distributions, which are manifested at the macroscopic level in the familiar exponential kinetics that have been measured for ensembles. The strength of single-molecule methods is their ability to detect molecular heterogeneity, transient intermediates, rare events and the sequence of events, all of which might be hidden in population-averaged measurements. Fluorescence methods can detect single molecules because of the high sensitivity afforded by optimized optics and fluorescent dyes, combined with efficient detectors and detection geometries. In addition, fluorescence resonance energy transfer (FRET) can serve as a

'spectroscopic ruler'⁴⁵, allowing characterization of distance over time when experiments are carried out in a time-resolved manner. One of the limitations of single-molecule FRET is that only a single distance change is measured. When higher-resolution structural information is available, however, these distance changes can be interpreted in terms of possible corresponding conformational changes.

The power of single-molecule FRET to unravel the detailed molecular mechanism of an important multisubunit enzyme was elegantly demonstrated by Diez and colleagues for F₀F₁-ATP synthase⁴⁶ (Fig. 3). This membrane-bound enzyme converts the electrochemical energy of a transmembrane proton gradient into chemical energy in the form of ATP. Using the intact protein complex in vesicles (liposomes), the stepwise rotation of the γ -subunit driven by the proton gradient was followed in real time by single-molecule FRET (Fig. 3). The slow diffusion of the particles, due to the size of the liposomes, allowed measurements over hundreds of milliseconds. Strikingly, the experiment captured several rotational steps between three distinct FRET levels in a specific order. The order of switching was reversed during ATP synthesis, relative to ATP hydrolysis. This heroic single-molecule FRET study provided insights into the mechanism of catalysis that could only be obtained by single-molecule experiments, owing to the consecutive and progressive nature of the dynamics involved. An important feature exposed by such single-molecule experiments is that the actual transition between the substates is fast (faster than the time resolution), whereas the observed 'slowness' of switching arises from the low probability of transitions (Fig. 3c).

Computational methods

Computation has the unbeatable edge in that it can describe protein dynamics completely: the precise position of each atom at any instant in time for a single protein molecule can be followed, along with the corresponding energies, provided that at least one high-resolution structure is known as a starting point. Although conformational substates (located in energy wells) and their rates of interconversion can be detected experimentally (as described earlier), an atomic-resolution structural description of the 'climb from one valley to another' (the transition pathway) is out of experimental reach, owing to the extremely low probability and short lifetime of the high-energy conformers. Computational methods would be able to overcome these limitations if a perfect description of the protein-solvent system could be provided by

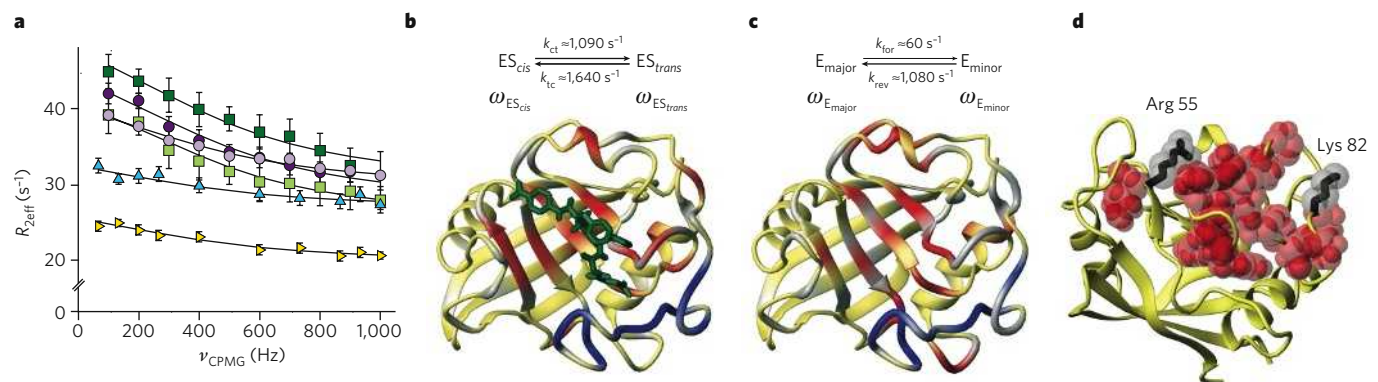


Figure 2 | Microsecond-to-millisecond protein dynamics are necessary for catalysis and are an intrinsic property of CYPA as shown by NMR relaxation dispersion experiments. a, Global fit of NMR relaxation data for representative ¹⁵N backbone amides and ¹³C methyl groups in CYPA (denoted by different shapes) during catalysis of the peptide *N*-succinyl-Ala-Phe-Pro-Phe-*p*-nitroanilide is shown. $R_{2\text{eff}}$ is the overall transverse relaxation rate, and ν_{CPMG} is the applied effective magnetic field. **b**, During catalysis of the peptide (green) by CYPA, residues undergoing conformational exchange at the rates shown in the reaction scheme are plotted on the structure (red). Residues in one loop (blue) undergo exchange at a faster rate. Residues for which there are no data are shown in grey. ES denotes enzyme with substrate, and ω denotes chemical shift. The rate constant for *cis* to *trans* isomerization is denoted k_{c} ; and for

trans to *cis* isomerization, k_{t} . **c**, Analysis of the free enzyme, E, reveals a striking correspondence in the residues undergoing exchange on a similar timescale. Moreover, agreement between the chemical-shift differences of the exchanging species (between $\omega_{\text{ES}_{\text{cis}}} - \omega_{\text{ES}_{\text{trans}}}$ and $\omega_{\text{E}_{\text{major}}} - \omega_{\text{E}_{\text{minor}}}$) implies that exchange occurs between the same two states in each case and that the substrate merely shifts a pre-existing equilibrium. The rate constants for the forward and reverse reaction are denoted k_{for} and k_{rev} , respectively. **d**, Residues that build a common dynamic network (displayed as van der Waals radii, red) were identified by measuring chemical-shift changes between the wild-type protein and mutant proteins in which either Arg 55 or Lys 82 was mutated to alanine (residues shown in black). These chemical-shift changes are caused simply by shifting the pre-existing equilibrium. (Figure reproduced, with permission, from ref. 36.)

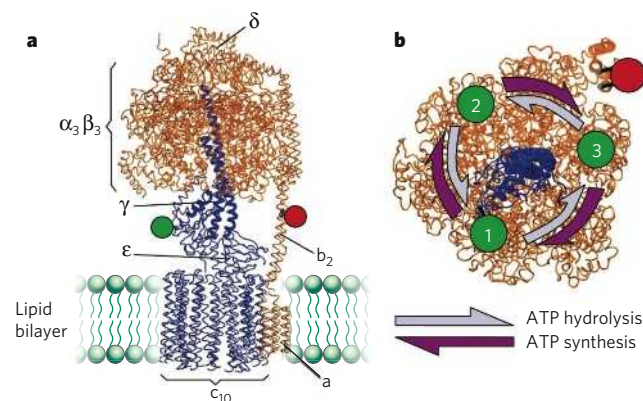
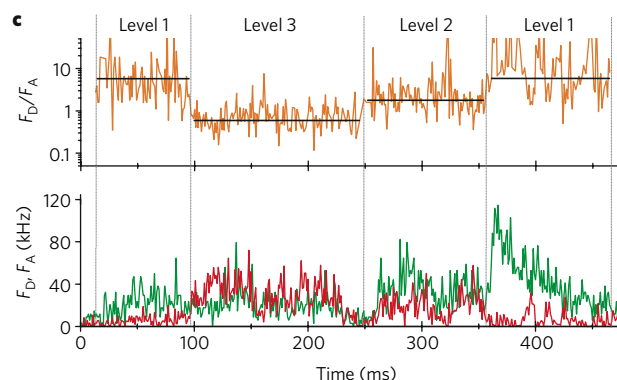


Figure 3 | Single-molecule FRET reveals ordered, stepwise rotation of F_0F_1 -ATP synthase on the millisecond timescale during ATP hydrolysis and synthesis. **a**, Model of F_0F_1 -ATP synthase embedded in a lipid bilayer. The rotor subunits are shown in blue, and the stator subunits are shown in orange. The FRET donor (green) is bound to the γ -subunit, and the FRET acceptor (red) is bound to the b-subunits. **b**, Cross-section at the level of the fluorophore, as viewed from the membrane. The change in position of the donor is shown relative to the acceptor on rotation of the rotor



subunits (blue) in 120° steps. **c**, Single-molecule time traces of a single F_0F_1 -ATP synthase molecule in liposomes during ATP hydrolysis. The fluorescence intensities (lower panel) of the donor (F_D , green) and the acceptor (F_A , red), as well as the corrected intensity ratio (F_D/F_A , upper panel, orange), uncover stepping between three states, with unique donor-acceptor distances in the order 1 \rightarrow 3 \rightarrow 2 \rightarrow 1 (which correspond to the numbers in part **b**). Data were collected over 1 ms intervals. (Figure reproduced, with permission, from ref. 46.)

the force field (that is, parameter sets describing the potential energy of all atoms). Impressive progress has been made in the development of these force fields since their original conception^{47,48}, and they are used in molecular-dynamics simulations^{47,49} (see the section Fast timescales).

Unfortunately, protein dynamics on the microsecond-to-millisecond timescale is currently out of reach for conventional molecular-dynamics simulations. To overcome this restriction, a large variety of approaches that simplify force fields have been developed, including normal mode analysis^{50,51}, gaussian network models⁵², FIRST (floppy inclusion and rigid substructure topography)⁵³, FRODA (framework rigidity optimized dynamic algorithm)⁵⁴ and Gō models⁴⁹. Alternatively, the dynamic process is accelerated by external force to access this timescale (used in methods such as targeted, steered and accelerated molecular-dynamics simulations^{47,55-57}), or prior knowledge about features of the reaction coordinate (umbrella sampling algorithms to construct a potential of mean force⁵⁸) or the transition end points (transition-path sampling⁵⁹) is necessary.

Knowledge of thousands of high-resolution protein structures, together with the growing accessibility of various computational methods, has resulted in a large body of computational studies of protein dynamics. Given the power of computation, on the one hand, and the stringent prerequisite for accurate energetic descriptions of the system (small energy differences must be calculated relative to the absolute sum of all energetic terms of the system), on the other hand, experimental

validation is necessary. Ideally, this should be an iterative process, with experimental testing of computational predictions and extensions of current computational methodology. This process is particularly important for tier-0 motions, because extensive approximations are required to gain access to this timescale computationally.

Fast timescales

'Fast' timescale dynamics (tier-1 and tier-2 dynamics) define fluctuations within the well of a tier-0 state. In contrast to the slow timescale, a large ensemble of structurally similar states that are separated by energy barriers of less than $1 kT$ result in more-local, small-amplitude picosecond-to-nanosecond fluctuations at physiological temperature (Fig. 1a). The interest in this timescale arises from the sampling of a large number of states, implicating these substates in the entropy of the system. In contrast to the tier-0 states, the large number of higher-tier states requires a statistical description of the distribution. We distinguish between tier-1 and tier-2 substates as small groups of atoms fluctuating collectively on the nanosecond timescale (such as loop motions) and local atomic fluctuations on the picosecond timescale (such as side-chain rotations), respectively (Fig. 1). We note that even higher tiers exist, such as femtosecond bond vibrations. Naturally, the structure dictates the features of atomic motion, with backbone atoms located in secondary structures being more restrained than atoms in loops. In this section, we discuss what has been learned about dynamics on the fast

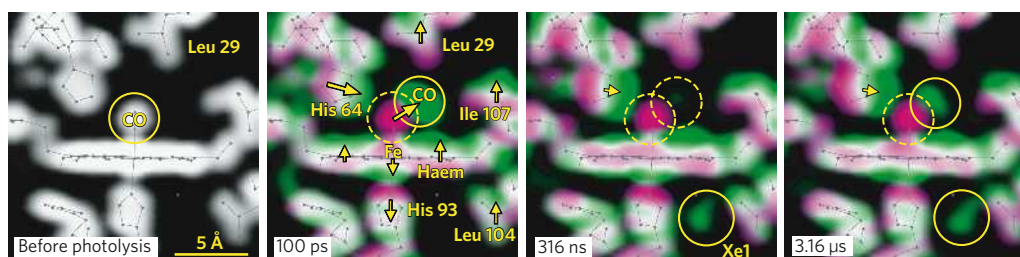


Figure 4 | Time dependence of carbon-monoxide migration and corresponding structural relaxation in myoglobin, using picosecond time-resolved X-ray crystallography. The ground-state electron density of carbon-monoxide (CO)-bound myoglobin is shown (left). Time-resolved changes after flash-photolysis-triggered dissociation of CO are displayed as coloured electron-density maps: the ground state is shown in pink, and the photolysed state in green; where these overlap, the colour blends to white. The direction of motion (indicated by arrows) follows the

gradient from pink to green. Sites occupied by CO are indicated by solid circles, and sites evacuated by CO are indicated by dashed circles. The photolysed CO is initially trapped in the primary docking site, about 2 \AA from the binding site and migrates subsequently to the xenon docking site Xe1 on the opposite side of the haem. Concurrent fast movements of active-site side chains (on the picosecond timescale) prevent immediate rebinding of CO. (Figure reproduced, with permission, from ref. 61.)

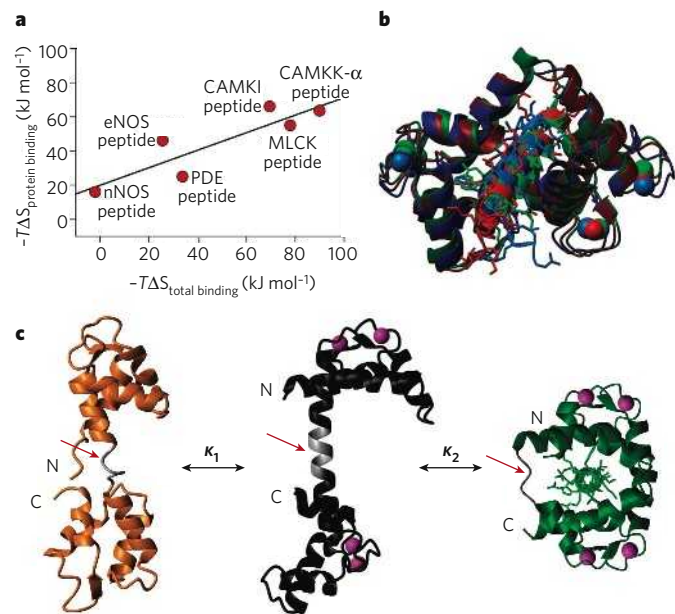


Figure 5 | The role of protein dynamics in molecular recognition by calmodulin on a range of timescales. a, Correlation between the change in conformational entropy of calmodulin ($\Delta S_{\text{protein binding}}$) and the change in total system entropy ($\Delta S_{\text{total binding}}$) on binding of peptides from target proteins. $\Delta S_{\text{protein binding}}$ was estimated from methyl-NMR order parameters, and $\Delta S_{\text{total binding}}$ was measured by isothermal titration calorimetry. (Panel reproduced, with permission, from ref. 72.) **b**, Overlay of X-ray crystal structures of calmodulin bound to several target peptides: calcium/calmodulin-dependent protein kinase I (CAMK1)-derived peptide (red); smooth-muscle myosin light-chain kinase (MLCK)-derived peptide (green); and endothelial nitric-oxide synthase (eNOS)-derived peptide (dark blue). Peptides bind in the centre of the structure (lighter shading). From this overlay, it is clear that there are large variations in the peptide side chains and consequently in the structure of calmodulin. Image generated from files from the PDB, based on data from the following: ref. 94, file 1MXE; ref. 95, file 1CDL; and ref. 96, file 1NIW. **c**, Mechanism of Ca^{2+} signalling and target recognition through coupled conformational equilibria. NMR experiments established that there is a dynamic equilibrium (K_1) between the structures of Ca^{2+} -free calmodulin (orange) and Ca^{2+} -bound calmodulin (black, Ca^{2+} in pink) in the absence of Ca^{2+} ; Ca^{2+} binding then shifts this equilibrium to the right⁷⁴. Further evidence from NMR spectroscopy indicates that the linker between the domains (grey, indicated by red arrows) remains flexible in the Ca^{2+} -bound state⁷⁵. We propose that peptide binding occurs through selective binding to a pre-existing conformation of calmodulin (K_2 equilibrium), which is similar to the experimentally observed structure shown in green. Images generated from files from the PDB, based on data from the following: ref. 97, file 1CFD (left); ref. 76, file 1CLL (centre); and ref. 95, file 1CDL (right). CAMKK- α , calcium/calmodulin-dependent protein kinase kinase 1 α ; nNOS, neural nitric-oxide synthase; PDE, phosphodiesterase.

timescale from experimental atomic-resolution methods, experimental low-resolution and local-site methods, and computational methods.

Experimental atomic-resolution methods

X-ray-diffraction data contain information not only about the average three-dimensional structure (tier-0 state) but also about the spatial distribution around this state (tier-1 and tier-2 states). This mean-square atomic displacement¹² is commonly expressed as the B factor (also known as the temperature factor and the Debye–Waller factor). Atomic displacement can originate from both static disorder (that is, an ensemble of substates present in solution are trapped in the crystal) and dynamic disorder (that is, fluctuations that occur in the crystal). Thus, B factors cannot be interpreted simply as the amplitude of atomic fluctuations, because both true intramolecular motion and lattice disorder contribute to them. In addition, crystal contacts affect B factors. Recent advances in X-ray technology have resulted in structural models with

sub-angstrom resolution, allowing novel insights into the directionality of atomic fluctuations through anisotropic B factors⁶⁰. Laue X-ray diffraction can measure the purely dynamic component, with the added advantage of delivering the timescale of motions¹⁹.

The elegance of Laue X-ray diffraction is illustrated by the time-resolved, high-resolution images that have been obtained for carbon-monoxide migration in myoglobin⁶¹, which has been called the hydrogen atom of biology⁶². The dissociation of carbon monoxide from the haem cofactor was triggered by flash photolysis, and the resultant structural rearrangements were followed in real time⁶¹ (Fig. 4). Clearly, correlated side-chain motions on the picosecond-to-nanosecond timescale coincide with carbon monoxide moving from its primary docking site into secondary pockets. This example highlights the role that angstrom-scale fast motions in the active site of myoglobin have in the reversible binding of the ligand, allowing a fast response to changes in the balance of oxygen and carbon monoxide in the blood. Unfortunately, this method cannot be universally applied to proteins, because the reaction needs to be triggered in the crystal and the structural changes must be small enough to be tolerated within the crystal lattice.

When using NMR relaxation methods, picosecond-to-nanosecond dynamics are characterized in terms of the amplitude (the order parameter, S^2 , does not include directionality) and the timescale (τ_c , the internal correlation time) of bond fluctuations. S^2 ranges from 0 (isotropic rotation) to 1 (completely rigid) and is commonly measured for backbone amide bonds and side-chain methyl groups²⁴. These local dynamics ('fast-timescale dynamics' in NMR-spectroscopy jargon) must be faster than the overall tumbling time of the protein to be detectable by solution NMR methods. In solid-state NMR spectroscopy, motions on a broader timescale (low microsecond and faster) can be detected^{63,64}. In addition, there is no protein size limit in solid-state NMR spectroscopy, but technical challenges remain to be solved before dynamics can be routinely measured at atomic resolution in large proteins.

Because these fast-timescale dynamics are, ultimately, connected to entropy, NMR spectroscopy has been used extensively to investigate the entropic contribution of the protein to biomolecular binding (in protein–protein, protein–DNA, protein–RNA and protein–other-ligand interactions)^{65–69}. Here, we use calmodulin to illustrate the advantages and limitations of this method for quantifying entropic contributions to affinity, because the natural function of calmodulin is to bind to a variety of target proteins. In the Ca^{2+} -bound form, the two domains clamp around the helical peptide-recognition sequence of target proteins (Fig. 5b, c). Although the free energy of binding is similar for Ca^{2+} -bound calmodulin interacting with many of these peptide sequences, the enthalpic and entropic contributions vary widely, as measured by isothermal titration calorimetry^{70–72}. Using NMR spectroscopy, Wand and collaborators⁷² identified differences in methyl order parameters of Ca^{2+} -bound calmodulin on binding to several peptide targets as contributing to this variation in entropy (Fig. 5a). However, the conversion of order parameters into absolute entropic energies is challenging and controversial^{65–69,72,73}. A trend correlating the entropy calculated from the methyl-NMR order parameters of calmodulin and the total binding entropy of the system obtained from isothermal titration calorimetry is observed⁷² (Fig. 5a), in agreement with the fact that many of these methyl groups line the peptide-binding pocket. Although the correlation is not strong, it is intriguing. This NMR method does not allow quantitative determination of the total protein entropy: only a subset of atoms is measured, and entropic changes in the peptides and solvent, which have not yet been characterized, might be major contributors to the total system entropy. The only component of the system that varies is the peptide itself, and a similar characterization of the peptides by NMR spectroscopy could be carried out. A comparison of known calmodulin–peptide structures exposes the differences in the calmodulin–peptide interfaces (Fig. 5b). Vastly different peptide side chains not only alter the packing of side chains with calmodulin but also displace the backbone of calmodulin. Packing shapes the amplitude and directionality of fluctuations, thus inspecting the structures should also allow insight into the entropic contribution to binding, as well as the enthalpic contribution of specific protein–peptide interactions.

The structural variation of these complexes raises the question of the mechanism of binding and specificity. The binding of Ca^{2+} to calmodulin was originally thought to induce activation through reorganization within each domain, but NMR relaxation experiments have revealed that the binding of Ca^{2+} shifts a pre-existing equilibrium⁷⁴. We propose that peptide binding also proceeds through such an equilibrium-shift mechanism (Fig. 5c). This is supported by several lines of evidence: NMR data indicate that the linker helix between the domains is flexible in the absence of peptide⁷⁵; X-ray diffraction has trapped both an extended structure (Protein Data Bank (PDB) identity 1CLL)⁷⁶ and a closed structure (PDB identity 1PRW)⁷⁷; and single-molecule FRET distributions show that a wide range of interdomain distances are sampled^{78,79}. This flexibility of calmodulin on the microsecond-to-millisecond timescale allows the ligands to select their preferred conformation, explaining the specificity of calmodulin for so many targets.

Experimental lower-resolution and local-site methods

Many of the low-resolution spectroscopic methods described in the section Slow timescales can also access this faster timescale. In addition, neutron scattering measures average root-mean-square fluctuations on any type of biological sample, thereby allowing dynamics to be characterized over a large temperature range. This method has demonstrated the influence of temperature and solvent conditions on the glass transition⁸⁰.

So far, we have discussed various timescales and their role in biological processes, but we have left out a fundamental motion: bond vibration on the femtosecond timescale. Advances in laser technology have initiated the fascinating era of femtosecond spectroscopy^{81,82}, and Zewail⁸² and co-workers have developed the field of four-dimensional, ultrafast electron diffraction, crystallography and microscopy. These methods have extended the experimentally accessible time range, allowing direct observation of the basic chemical steps in enzymes: the breaking and forming of bonds, and the transfer of protons, hydride ions and electrons.

Computational methods

The most fundamental description of a system is computed using quantum mechanics, with molecular mechanics and molecular dynamics progressively simplifying the calculations to allow dynamics simulations on protein systems^{2,47,49}. Tier-1 and tier-2 dynamics are on a perfect timescale for molecular-dynamics simulations. One of the advantages of molecular-dynamics simulations is that correlations between motions can be disentangled, a phenomenon that is obscured in experiments on ensembles. Most importantly, although experiments can determine what is moving and how fast, molecular-dynamics simulations can answer why things move, because the underlying forces and corresponding energies are included in the simulation. The resultant predictions inspire new experiments, forming part of a combined effort to solve the puzzle of how proteins work.

This point is exemplified by the problem of ion selectivity in potassium channels. How can a channel make a 'hole' in the membrane that allows ions to diffuse rapidly (10^8 ions per second) but discriminate 1,000-fold for K^+ over Na^+ , which is only 0.4 Å smaller? The breakthrough crystal structure of a potassium channel, KcsA from *Streptomyces lividans* (PDB identity 1BL8)⁸³, provided unprecedentedly detailed structural information (Fig. 6a) and an immediate answer to this question. A narrow region of the pore, the selectivity filter, was perfectly sized to coordinate dehydrated K^+ but too large for dehydrated Na^+ : the authors of this study concluded that "The structure of the selectivity filter with its molecular springs holding it open prevents the carbonyl oxygen atoms from approaching close enough to compensate for the cost of dehydration of a Na^+ ion"⁸³. However, solution NMR spectroscopy shows increased flexibility in the selectivity filter relative to the transmembrane helices⁸⁴. In addition, molecular-dynamics simulations on this structure of KcsA in a fully solvated lipid membrane show fluctuations of the selectivity filter over a range of ion-carbonyl distances that are sufficient to coordinate either ion⁸⁵ (Fig. 6b).

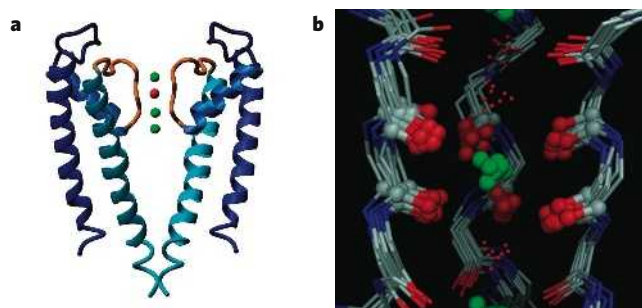


Figure 6 | Ion-channel selectivity investigated by X-ray crystallography and molecular-dynamics simulations. **a**, X-ray crystal structure of the potassium-selective channel KcsA. The structure has four subunits that create a central pore for ion conductance; for clarity, only two subunits are shown. The narrowest part of the pore was identified as the selectivity filter (orange). This region contains four ion-binding sites, in which backbone carbonyl groups coordinate K^+ ions perfectly. Three ions (green) and one water molecule (red) were observed in the selectivity filter. Image generated from file 1BL8 from the PDB, based on data from ref. 83. **b**, Superposition of snapshots of the selectivity filter from molecular-dynamics simulations. For clarity, only three subunits are shown. A K^+ ion (green) is coordinated in the S2 site by eight backbone carbonyl groups (six shown, with oxygen atoms depicted as large red spheres). Water molecules (small red circles) occupy adjacent sites. Atomic fluctuations of the selectivity filter on the order of 0.5–1 Å are captured in the molecular-dynamics trajectories. Nitrogen atoms are shown in blue, and carbon atoms are shown in grey. (Panel reproduced, with permission, from ref. 98.)

Importantly, this flexibility seems not to eliminate selectivity. The authors of the molecular-dynamics-simulation study⁸⁵ suggest that selectivity is controlled by the intrinsic electrostatic properties of the coordinating carbonyl groups and not by the average size of the pore measured by crystallography. Ultimately, selectivity is determined by the free-energy difference between K^+ and Na^+ partitioning between bulk water and the pore. The number of the coordinating groups, their nature and their distance distribution to the respective ion all contribute to this free-energy difference. To resolve the remaining controversies, the relative contributions of these factors need to be characterized precisely.

The hierarchy in space and time

In the previous sections, dynamics were separated into different timescales to discuss methodology, as well as examples that illustrate individual aspects of protein dynamics. However, a comprehensive description of the energy landscape requires connection between different timescales and the corresponding amplitudes of motions (Fig. 1a). Moreover, the ultimate goal is to understand how proteins function in real time. To live up to this task, several of the methods described here must be combined. This concept is illustrated using adenylate kinase (Fig. 7), an enzyme that catalyses the reversible conversion of an ATP and an AMP molecule into two ADP molecules.

Large conformational changes between the substrate-free enzyme and the substrate-bound enzyme have been observed⁸⁶ (Fig. 7a). Using ¹⁵N-NMR relaxation experiments^{34,39,40} on the turning-over enzyme, our research group showed that opening of the nucleotide 'lids', and not phosphotransfer, is the rate-limiting step for overall turnover⁸⁷. Interestingly, comparison of the protein dynamics of a hyperthermophilic adenylate kinase (thermoAdk) and a mesophilic adenylate kinase (meso-Adk) showed that the reduced catalytic activity of thermoAdk at ambient temperature is solely due to slower lid opening⁸⁷.

X-ray structures of free and substrate-bound adenylate kinases suggest the standard view of ligand-induced conformational change⁸⁶. However, the combined crystallographic, NMR spectroscopy, single-molecule and computational studies demand a fundamentally different picture⁸⁸. The first hint came from observing three distinct conformations within the asymmetric unit of substrate-free thermoAdk (Fig. 7a). Remarkably, these trapped substates lie along the trajectory towards the closed

state. Because X-ray-crystallographic structures reveal high-resolution snapshots but do not provide the probability of sampling these states and other states, nor the rates of transition between them, we used NMR spectroscopy to measure the dynamics in solution. Indeed, collective conformational exchange with a common rate constant of about 1 ms was detected⁸⁸, but the data did not allow determination of the structural nature of the motion.

Molecular-dynamics simulations were therefore carried out for substrate-free Adk in explicit water (that is, individual water molecules were included in the simulation) to connect the spatial (X-ray) and

kinetic (NMR spectroscopy) characteristics. The largest displacements occur in the nucleotide lids (Fig. 7b), and interconversion of the states observed in the three X-ray snapshots was reached within the 10 ns simulation time. If the fluctuations captured in the crystal happen on the nanosecond timescale, what process is detected on the millisecond timescale by NMR spectroscopy? Single-molecule FRET experiments on thermoAdk shed light on this question (Fig. 7d). Surprisingly, transitions between states that have dye–dye distances consistent with the fully open and fully closed states were detected for the free enzyme, highlighting the unique capability of single-molecule experiments to measure kinetics

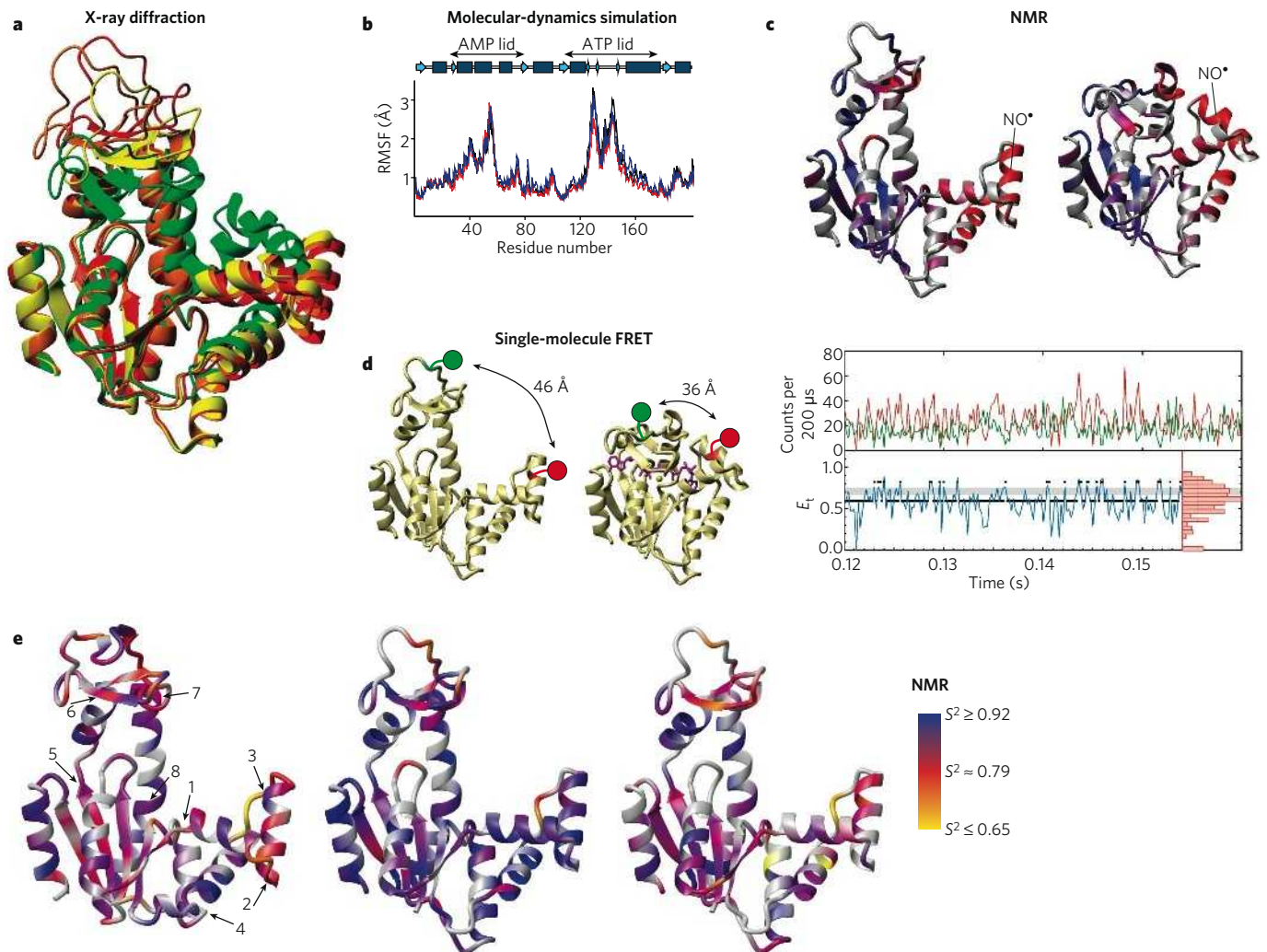


Figure 7 | A hierarchy of protein dynamics in space and time underlies enzyme catalysis, using the enzyme adenylate kinase as an example. **a**, The X-ray crystal structure of substrate-free thermoAdk captures snapshots along the trajectory towards the fully closed state. Molecules A, B and C in the asymmetric unit are shown in red, orange and yellow, respectively. The X-ray structure of thermoAdk bound to the bisubstrate analogue 5-di-adenosine-5'-pentaphosphate (green, substrate omitted for clarity) is superimposed. **b**, Root-mean-square fluctuations (RMSF) from 10-ns molecular-dynamics simulations of substrate-free thermoAdk molecules A, B and C (blue, red and black, respectively) show that the nucleotide lids are the most dynamic elements. A diagram of the secondary-structure elements is also shown, with α -helices indicated in dark blue and β -strands indicated in light blue (top). **c**, NMR paramagnetic relaxation enhancement (PRE) by a spin label (NO^{*}) attached to residue 52. Substrate-free thermoAdk (left) samples conformations resembling the fully closed state (right). The PRE-derived distances for substrate-free thermoAdk are plotted onto the structures as a continuous colour scale from dark blue (distant, small effect) to red (close, large effect). Residues for which there are no data are shown in grey. **d**, Individual opening and closing events monitored by time-resolved single-molecule FRET of substrate-free immobilized thermoAdk.

The positions of the FRET donor (green) and the FRET acceptor (red) on thermoAdk are indicated. The fluorescence intensities (upper panel of graph, green and red; colours correspond to donor and acceptor) are shown together with the corresponding FRET efficiencies (E_t , lower panel), including the E_t histogram (right). Each E_t value was assigned to either the open state (E_t below the grey band) or the closed state (E_t above the grey band) as indicated by black dots. **e**, NMR relaxation analysis of mesoAdk and thermoAdk. Fast (picosecond-to-nanosecond) atomic fluctuations are the physical origin of larger amplitude, slower nucleotide-lid motions. Order parameters (S^2) calculated from NMR relaxation data for mesoAdk at 20 °C (left) and thermoAdk at 20 °C (centre) and 80 °C (right) are shown as a continuous colour scale, with grey indicating proline residues and residues for which S^2 cannot be measured. The hinges are numbered and indicated with arrows. Importantly, at 20 °C, the picosecond-to-nanosecond hinge flexibility in mesoAdk is greater than in thermoAdk, and at this temperature, mesoAdk is known to be more active. In addition, the hinge flexibility on this timescale is similar in mesoAdk at 20 °C and thermoAdk at 80 °C, conditions in which both forms of the enzyme have similar activity. (Panel a–d reproduced, with permission, from ref. 88. Panel e reproduced, with permission, from ref. 89.)

when the spontaneous nature of the fluctuations impedes synchronization. Strikingly, the lifetime distributions of the open and closed states result in calculated rates that are in good agreement with the NMR rates measured for the ensemble. NMR paramagnetic relaxation enhancement, a powerful distance measure, unambiguously demonstrated sampling of a closed state. Severe line broadening was observed for residues that are far from the spin label in the open state but close to the spin label in the closed state (Fig. 7c). Thus, catalytically necessary conformational substates are already sampled in the free enzyme through motions with preferred directionality.

Turnover happens on the timescale of these tier-0, collective, large-amplitude motions. However, small-amplitude atomic thermal fluctuations occur on the picosecond timescale. How are these dynamic ranges connected? The link between these timescales was revealed by comparative analysis of thermoAdk and mesoAdk, using NMR spectroscopy and molecular-dynamics simulations⁸⁹. Increased picosecond dynamics were observed in the same places where the local backbone conformation must change for lid closure to occur (Fig. 7e). Moreover, these hinges are more flexible in mesoAdk than thermoAdk at low temperature, with thermoAdk achieving similar hinge dynamics at temperatures at which the catalytic activity matches that of mesoAdk at ambient temperatures. This striking correspondence suggests that the physical origin of the catalytically important collective domain motions (microseconds to milliseconds) is the fast-timescale (picoseconds to nanoseconds) local hinge motions. Differences in the fast hinge fluctuations are encoded by differences in the amino-acid sequence, leading to increased packing and rigidification of thermoAdk on the picosecond-to-nanosecond timescale.

This example illustrates how the hierarchy of protein dynamics in space and time arises from the protein structure encoded by the amino-acid sequence and is ultimately connected to enzyme function. Tier-0 transitions are improbable, and therefore slow, events that arise from many individual attempts by local groups to overcome the energy barrier. The low success rate results from the collective nature of these large-scale motions.

From physics to biology and vice versa

From electrons and nuclei by way of X-rays, radio waves, light waves and energy potentials to a high-energy teenager surfing waves or the Internet — what is the connection? Biological function is ultimately rooted in the physical motions of biomolecules. Many biological processes are controlled by alterations in rates and relative populations rather than by a simple ‘on-off’ switch. For example, enzymes speed up chemical reactions, and changes in intracellular ion concentrations trigger complex neurological processes. Considering the immense rate enhancements and equilibrium shifts that are achieved in biological systems, it is easy to overlook the fact that only small changes in free energy (around a few kT) account for these effects, owing to the exponential dependence of both the rate and the populations on the free-energy difference. In other words, the breaking of a few hydrogen bonds or van der Waals contacts in a protein, which contains hundreds to thousands of such interactions, can turn on a signalling cascade or catalyse a chemical reaction. Importantly, intrinsic protein dynamics can happen only in this free-energy range of several kT .

Because biological function is the property selected by evolution, we propose that the conformational substates sampled by a protein, and the pathways between them, are not random but rather a result of the evolutionary selection of states that are needed for protein function. Signal transduction, enzyme catalysis and protein–ligand interactions occur as a result of the binding of specific ligands to complementary pre-existing states of a protein and the consequent shifts in the equilibria^{26,35,36,75–79,90–92} (Fig. 1a). In other words, the dynamic landscape is an intrinsic property (or ‘personality’) of a protein and is encoded in its fold, and the ligand does not induce the formation of a new structure but, instead, selects a pre-existing structure.

The energy-landscape concept provides a vital bridge between the different philosophies and language used by physicists and biologists. For the field of biology to progress, quantitative analysis and the discovery

of fundamental unifying principles, which are both characteristic of physics, are required. Conversely, the complexity of the living world provides a challenging task for physicists. It can only be imagined where this marriage of biology and physics might lead. Here, we pose a few immediate and well-defined questions about protein dynamics. How does a protein move from one energy valley into another — what is the pathway(s), and what is the transition state(s)? What are the entropic and enthalpic factors that contribute to transition barriers? Can minor conformational substates be predicted from known structures? Other important questions facing the field include how this knowledge can be used to design novel proteins that have desired properties and whether a dynamic view of proteins can be used to help discover and develop novel therapeutic agents.

Although there is certainly nothing wrong with having one eye on potential applications, many of the greatest advances in science have been unforeseen outcomes of basic discoveries, sparked solely by scientific curiosity. The beauty of scientific adventure is this unpredictable journey as a scientific community, following new instincts and evolving new directions. ■

1. Chandler, D. Roles of classical dynamics and quantum dynamics on activated processes occurring in liquids. *J. Stat. Phys.* **42**, 49–67 (1986).
2. Olsson, M. H. M., Parson, W. W. & Warshel, A. Dynamical contributions to enzyme catalysis: critical tests of a popular hypothesis. *Chem. Rev.* **106**, 1737–1756 (2006).
3. Benkovic, S. J. & Hammes-Schiffer, S. A perspective on enzyme catalysis. *Science* **301**, 1196–1202 (2003).
4. Gertner, B. J., Wilson, K. R. & Hynes, J. T. Nonequilibrium solvation effects on reaction-rates for model S_N2 reactions in water. *J. Chem. Phys.* **90**, 3537–3558 (1989).
5. Schliwa, M. (ed.) *Molecular Motors* (Wiley, Weinheim, 2003).
6. Kolomeisky, A. B. & Fisher, M. E. Molecular motors: a theorist's perspective. *Annu. Rev. Phys. Chem.* **58**, 675–695 (2007).
7. Lazaridis, T. & Karplus, M. 'New view' of protein folding reconciled with the old through multiple unfolding simulations. *Science* **278**, 1928–1931 (1997).
8. Leopold, P. E., Montal, M. & Onuchic, J. N. Protein folding funnels — a kinetic approach to the sequence structure relationship. *Proc. Natl Acad. Sci. USA* **89**, 8721–8725 (1992).
9. Wolynes, P. G. Recent successes of the energy landscape theory of protein folding and function. *Q. Rev. Biophys.* **38**, 405–410 (2005).
10. Austin, R. H., Beeson, K. W., Eisenstein, L., Frauenfelder, H. & Gunsalus, I. C. Dynamics of ligand binding to myoglobin. *Biochemistry* **14**, 5355–5373 (1975).
11. Frauenfelder, H., Sligar, S. G. & Wolynes, P. G. The energy landscapes and motions of proteins. *Science* **254**, 1598–1603 (1991).
12. Frauenfelder, H., Petsko, G. A. & Tsernoglou, D. Temperature-dependent X-ray diffraction as a probe of protein structural dynamics. *Nature* **280**, 558–563 (1979).
13. Brooks, C. L. & Karplus, M. Solvent effects on protein motion and protein effects on solvent motion — dynamics of the active-site region of lysozyme. *J. Mol. Biol.* **208**, 159–181 (1989).
14. Fenimore, P. W., Frauenfelder, H., McMahon, B. H. & Parak, F. G. Slaving: solvent fluctuations dominate protein dynamics and functions. *Proc. Natl Acad. Sci. USA* **99**, 16047–16051 (2002).
15. Beece, D. et al. Solvent viscosity and protein dynamics. *Biochemistry* **19**, 5147–5157 (1980).
16. Fenimore, P. W., Frauenfelder, H., McMahon, B. H. & Young, R. D. Bulk-solvent and hydration-shell fluctuations, similar to α - and β -fluctuations in glasses, control protein motions and functions. *Proc. Natl Acad. Sci. USA* **101**, 14408–14413 (2004).
17. Shakhnovich, E. Protein folding thermodynamics and dynamics: where physics, chemistry, and biology meet. *Chem. Rev.* **106**, 1559–1588 (2006).
18. Lindorff-Larsen, K., Rogen, P., Paci, E., Vendruscolo, M. & Dobson, C. M. Protein folding and the organization of the protein topology universe. *Trends Biochem. Sci.* **30**, 13–19 (2005).
19. Bourgeois, D. & Royant, A. Advances in kinetic protein crystallography. *Curr. Opin. Struct. Biol.* **15**, 538–547 (2005).
20. Schlichting, I. et al. The catalytic pathway of cytochrome P450cam at atomic resolution. *Science* **287**, 1615–1622 (2000).
21. Englander, S. W. Hydrogen exchange and mass spectrometry: a historical perspective. *J. Am. Soc. Mass Spectrom.* **17**, 1481–1489 (2006).
22. Bai, Y. W. Protein folding pathways studied by pulsed- and native-state hydrogen exchange. *Chem. Rev.* **106**, 1757–1768 (2006).
23. Mittermaier, A. & Kay, L. E. New tools provide new insights in NMR studies of protein dynamics. *Science* **312**, 224–228 (2006).
24. Kay, L. E. NMR studies of protein structure and dynamics. *J. Magn. Reson.* **173**, 193–207 (2005).
25. Palmer, A. G. NMR characterization of the dynamics of biomacromolecules. *Chem. Rev.* **104**, 3623–3640 (2004).
26. Kern, D., Eisenmesser, E. Z. & Wolf-Watz, M. Enzyme dynamics during catalysis measured by NMR spectroscopy. *Methods Enzymol.* **394**, 507–524 (2005).
27. Pervushin, K., Riek, R., Wider, G. & Wuthrich, K. Attenuated T-2 relaxation by mutual cancellation of dipole-dipole coupling and chemical shift anisotropy indicates an avenue to NMR structures of very large biological macromolecules in solution. *Proc. Natl Acad. Sci. USA* **94**, 12366–12371 (1997).
28. Sprangers, R., Gribun, A., Hwang, P. M., Houry, W. A. & Kay, L. E. Quantitative NMR spectroscopy of supramolecular complexes: dynamic side pores in ClpP are important for product release. *Proc. Natl Acad. Sci. USA* **102**, 16678–16683 (2005).
29. Palmer, A. G., Grey, M. J. & Wang, C. Y. Solution NMR spin relaxation methods for characterizing chemical exchange in high-molecular-weight systems. *Methods Enzymol.* **394**, 430–465 (2005).

30. Tugarinov, V. & Kay, L. E. Quantitative C-13 and H-2 NMR relaxation studies of the 723-residue enzyme malate synthase G reveal a dynamic binding interface. *Biochemistry* **44**, 15970–15977 (2005).
31. Sprangers, R. & Kay, L. E. Quantitative dynamics and binding studies of the 20S proteasome by NMR. *Nature* **445**, 618–622 (2007).
32. Horst, R. *et al.* Direct NMR observation of a substrate protein bound to the chaperonin GroEL. *Proc. Natl Acad. Sci. USA* **102**, 12748–12753 (2005).
33. Christodoulou, J. *et al.* Heteronuclear NMR investigations of dynamic regions of intact *Escherichia coli* ribosomes. *Proc. Natl Acad. Sci. USA* **101**, 10949–10954 (2004).
34. Loria, J. P., Rance, M. & Palmer, A. G. A relaxation-compensated Carr–Purcell–Meiboom–Gill sequence for characterizing chemical exchange by NMR spectroscopy. *J. Am. Chem. Soc.* **121**, 2331–2332 (1999).
35. Eisenmesser, E. Z., Bosco, D. A., Akke, M. & Kern, D. Enzyme dynamics during catalysis. *Science* **295**, 1520–1523 (2002).
36. Eisenmesser, E. Z. *et al.* Intrinsic dynamics of an enzyme underlies catalysis. *Nature* **438**, 117–121 (2005).
37. Fischer, G., Wittmannliedob, B., Lang, K., Kiefhaber, T. & Schmid, F. X. Cyclophilin and peptidyl-prolyl *cis-trans* isomerase are probably identical proteins. *Nature* **337**, 476–478 (1989).
38. Takahashi, N., Hayano, T. & Suzuki, M. Peptidyl-prolyl *cis-trans* isomerase is the cyclosporin-A-binding protein cyclophilin. *Nature* **337**, 473–475 (1989).
39. Loria, J. P., Rance, M. & Palmer, A. G. A TROSY CPMG sequence for characterizing chemical exchange in large proteins. *J. Biomol. NMR* **15**, 151–155 (1999).
40. Tollinger, M., Skrynnikov, N. R., Mulder, F. A. A., Forman-Kay, J. D. & Kay, L. E. Slow dynamics in folded and unfolded states of an SH3 domain. *J. Am. Chem. Soc.* **123**, 11341–11352 (2001).
41. Michalet, X., Weiss, S. & Jager, M. Single-molecule fluorescence studies of protein folding and conformational dynamics. *Chem. Rev.* **106**, 1785–1813 (2006).
42. Myong, S., Stevens, B. C. & Ha, T. Bridging conformational dynamics and function using single-molecule spectroscopy. *Structure* **14**, 633–643 (2006).
43. Yang, H. *et al.* Protein conformational dynamics probed by single-molecule electron transfer. *Science* **302**, 262–266 (2003).
44. Deniz, A. A., Mukhopadhyay, S. & Lemke, E. A. Single-molecule biophysics: at the interface of biology, physics and chemistry. *J. R. Soc. Interface* advance online publication, doi:10.1098/rsif.2007.1021 (22 May 2007).
45. Stryer, L. & Haugland, R. P. Energy transfer — a spectroscopic ruler. *Proc. Natl Acad. Sci. USA* **58**, 719–726 (1967).
46. Diez, M. *et al.* Proton-powered subunit rotation in single membrane-bound F_1F_0 -ATP synthase. *Nature Struct. Mol. Biol.* **11**, 135–141 (2004).
47. Adcock, S. A. & McCammon, J. A. Molecular dynamics: survey of methods for simulating the activity of proteins. *Chem. Rev.* **106**, 1589–1615 (2006).
48. McCammon, J. A., Gelin, B. R. & Karplus, M. Dynamics of folded proteins. *Nature* **267**, 585–590 (1977).
49. Scheraga, H. A., Khalili, M. & Liwo, A. Protein-folding dynamics: overview of molecular simulation techniques. *Annu. Rev. Phys. Chem.* **58**, 57–83 (2007).
50. Karplus, M. & Kushick, J. N. Method for estimating the configurational entropy of macromolecules. *Macromolecules* **14**, 325–332 (1981).
51. Ma, J. P. & Karplus, M. Ligand-induced conformational changes in *ras* p21: a normal mode and energy minimization analysis. *J. Mol. Biol.* **274**, 114–131 (1997).
52. Haliloglu, T., Bahar, I. & Erman, B. Gaussian dynamics of folded proteins. *Phys. Rev. Lett.* **79**, 3090–3093 (1997).
53. Jacobs, D. J., Rader, A. J., Kuhn, L. A. & Thorpe, M. F. Protein flexibility predictions using graph theory. *Proteins* **44**, 150–165 (2001).
54. Wells, S., Menor, S., Hespeneide, B. & Thorpe, M. F. Constrained geometric simulation of diffusive motion in proteins. *Phys. Biol.* **2**, S127–S136 (2005).
55. Hamelberg, D., Mongan, J. & McCammon, J. A. Accelerated molecular dynamics: a promising and efficient simulation method for biomolecules. *J. Chem. Phys.* **120**, 11919–11929 (2004).
56. Paci, E. & Karplus, M. Forced unfolding of fibronectin type 3 modules: an analysis by biased molecular dynamics simulations. *J. Mol. Biol.* **288**, 441–459 (1999).
57. Schlitter, J., Engels, M., Kruger, P., Jacoby, E. & Wollmer, A. Targeted molecular-dynamics simulation of conformational change — application to the T–R transition in insulin. *Mol. Simul.* **10**, 291–308 (1993).
58. Roux, B. The calculation of the potential of mean force using computer simulations. *Comput. Phys. Commun.* **91**, 275–282 (1995).
59. Dellago, C. & Bolhuis, P. G. Transition path sampling simulations of biological systems. *Top. Curr. Chem.* **268**, 291–317 (2007).
60. Merritt, E. A. Expanding the model: anisotropic displacement parameters in protein structure refinement. *Acta Crystallogr. D Biol. Crystallogr.* **55**, 1109–1117 (1999).
61. Schotte, F., Soman, J., Olson, J. S., Wulff, M. & Anfinsen, P. A. Picosecond time-resolved X-ray crystallography: probing protein function in real time. *J. Struct. Biol.* **147**, 235–246 (2004).
62. Frauenfelder, H., McMahon, B. H. & Fenimore, P. W. Myoglobin: the hydrogen atom of biology and a paradigm of complexity. *Proc. Natl Acad. Sci. USA* **100**, 8615–8617 (2003).
63. Franks, W. T. *et al.* Magic-angle spinning solid-state NMR spectroscopy of the $\beta 1$ immunoglobulin binding domain of protein G (GB1): N-15 and C-13 chemical shift assignments and conformational analysis. *J. Am. Chem. Soc.* **127**, 12291–12305 (2005).
64. Lorieau, J. L. & McDermott, A. E. Conformational flexibility of a microcrystalline globular protein: order parameters by solid-state NMR spectroscopy. *J. Am. Chem. Soc.* **128**, 11505–11512 (2006).
65. Akke, M., Bruschweiler, R. & Palmer, A. G. NMR order parameters and free-energy — an analytical approach and its application to cooperative Ca^{2+} binding by calbindin- D_{9k} . *J. Am. Chem. Soc.* **115**, 9832–9833 (1993).
66. Jarymowycz, V. A. & Stone, M. J. Fast time scale dynamics of protein backbones: NMR relaxation methods, applications, and functional consequences. *Chem. Rev.* **106**, 1624–1671 (2006).
67. Lee, A. L., Sharp, K. A., Kranz, J. K., Song, X. J. & Wand, A. J. Temperature dependence of the internal dynamics of a calmodulin–peptide complex. *Biochemistry* **41**, 13814–13825 (2002).
68. Li, Z. G., Raychaudhuri, S. & Wand, A. J. Insights into the local residual entropy of proteins provided by NMR relaxation. *Protein Sci.* **5**, 2647–2650 (1996).
69. Yang, D. W. & Kay, L. E. Contributions to conformational entropy arising from bond vector fluctuations measured from NMR-derived order parameters: application to protein folding. *J. Mol. Biol.* **263**, 369–382 (1996).
70. Brox, R. D., Lopez, M. M., Vogel, H. J. & Makhatazde, G. I. Energetics of target peptide binding by calmodulin reveals different modes of binding. *J. Biol. Chem.* **276**, 14083–14091 (2001).
71. Wintrose, P. L. & Privalov, P. L. Energetics of target peptide recognition by calmodulin: a calorimetric study. *J. Mol. Biol.* **266**, 1050–1062 (1997).
72. Frederick, K. K., Marlow, M. S., Valentine, K. G. & Wand, A. J. Conformational entropy in molecular recognition by proteins. *Nature* **448**, 325–329 (2007).
73. Best, R. B., Clarke, J. & Karplus, M. What contributions to protein side-chain dynamics are probed by NMR experiments? A molecular dynamics simulation analysis. *J. Mol. Biol.* **349**, 185–203 (2005).
74. Evenas, J., Forsen, S., Malmendal, A. & Akke, M. Backbone dynamics and energetics of a calmodulin domain mutant exchanging between closed and open conformations. *J. Mol. Biol.* **289**, 603–617 (1999).
75. Barbato, G., Ikura, M., Kay, L. E., Pastor, R. W. & Bax, A. Backbone dynamics of calmodulin studied by N-15 relaxation using inverse detected 2-dimensional NMR-spectroscopy — the central helix is flexible. *Biochemistry* **31**, 5269–5278 (1992).
76. Chattopadhyaya, R., Meador, W. E., Means, A. R. & Quioco, F. A. Calmodulin structure refined at 1.7 angstrom resolution. *J. Mol. Biol.* **228**, 1177–1192 (1992).
77. Fallon, J. L. & Quioco, F. A. A closed compact structure of native Ca^{2+} -calmodulin. *Structure* **11**, 1303–1307 (2003).
78. Johnson, C. K. Calmodulin, conformational states, and calcium signaling. A single-molecule perspective. *Biochemistry* **45**, 14233–14246 (2006).
79. Torok, K., Tzortzopoulos, A., Grabarek, Z., Best, S. L. & Thorogate, R. Dual effect of ATP in the activation mechanism of brain Ca^{2+} /calmodulin-dependent protein kinase II by Ca^{2+} /calmodulin. *Biochemistry* **40**, 14878–14890 (2001).
80. Doster, W., Cusack, S. & Petry, W. Dynamical transition of myoglobin revealed by inelastic neutron scattering. *Nature* **337**, 754–756 (1989).
81. Zhong, D. S. Ultrafast catalytic processes in enzymes. *Curr. Opin. Chem. Biol.* **11**, 174–181 (2007).
82. Zewail, A. H. 4D ultrafast electron diffraction, crystallography, and microscopy. *Annu. Rev. Phys. Chem.* **57**, 65–103 (2006).
83. Doyle, D. A. *et al.* The structure of the potassium channel: molecular basis of K^+ conduction and selectivity. *Science* **280**, 69–77 (1998).
84. Chill, J. H., Louis, J. M., Baber, J. L. & Bax, A. Measurement of ^{15}N relaxation in the detergent-solubilized tetrameric KcsA potassium channel. *J. Biomol. NMR* **36**, 123–136 (2006).
85. Noskov, S. Y., Berneche, S. & Roux, B. Control of ion selectivity in potassium channels by electrostatic and dynamic properties of carbonyl ligands. *Nature* **431**, 830–834 (2004).
86. Vonrhein, C., Schluederger, G. J. & Schulz, G. E. Movie of the structural changes during a catalytic cycle of nucleoside monophosphate kinases. *Structure* **3**, 483–490 (1995).
87. Wolf-Watz, M. *et al.* Linkage between dynamics and catalysis in a thermophilic-mesophilic enzyme pair. *Nature Struct. Mol. Biol.* **11**, 945–949 (2004).
88. Henzler-Wildman, K. A. *et al.* Intrinsic motions along an enzymatic reaction trajectory. *Nature* **450**, 838–844 (2007).
89. Henzler-Wildman, K. A. *et al.* A hierarchy of timescales in protein dynamics is linked to enzyme catalysis. *Nature* **450**, 913–916 (2007).
90. Volkman, B. F., Lipson, D., Wemmer, D. E. & Kern, D. Two-state allosteric behavior in a single-domain signaling protein. *Science* **291**, 2429–2433 (2001).
91. Tsai, C. J., Kumar, S., Ma, B. & Nussinov, R. Folding funnels, binding funnels, and protein function. *Protein Sci.* **8**, 1181–1190 (1999).
92. Boehr, D. D., Dyson, H. J. & Wright, P. E. An NMR perspective on enzyme dynamics. *Chem. Rev.* **106**, 3055–3079 (2006).
93. Ansari, A. *et al.* Protein states and protein quakes. *Proc. Natl Acad. Sci. USA* **82**, 5000–5004 (1985).
94. Clapperton, J. A., Martin, S. R., Smerdon, S. J., Gambin, S. J. & Bayley, P. M. Structure of the complex of calmodulin with the target sequence of calmodulin-dependent protein kinase I: studies of the kinase activation mechanism. *Biochemistry* **41**, 14669–14679 (2002).
95. Meador, W. E., Means, A. R. & Quioco, F. A. Target enzyme recognition by calmodulin — 2.4-angstrom structure of a calmodulin–peptide complex. *Science* **257**, 1251–1255 (1992).
96. Aoyagi, M., Arvai, A. S., Tainer, J. A. & Getzoff, E. D. Structural basis for endothelial nitric oxide synthase binding to calmodulin. *EMBO J.* **22**, 766–775 (2003).
97. Kubonawa, H. *et al.* Solution structure of calcium-free calmodulin. *Nature Struct. Biol.* **2**, 768–776 (1995).
98. Noskov, S. Y. & Roux, B. Ion selectivity in potassium channels. *Biophys. Chem.* **124**, 279–291 (2006).

Acknowledgements We thank M. Börsch, P. Anfinsen and B. Roux for providing the original images of Figs 3, 4 and 6b.

Author information Reprints and permissions information is available at npg.nature.com/reprints. Correspondence should be addressed to D.K. (dkern@brandeis.edu).